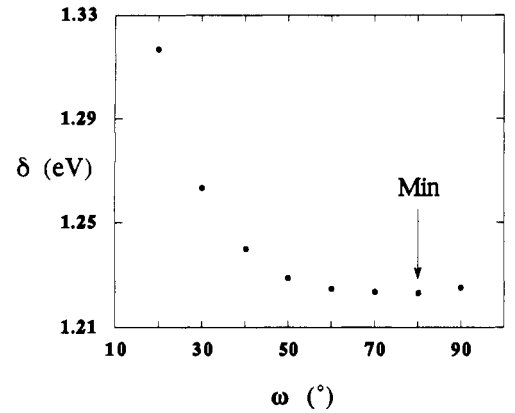

Figure 6. Variation of the energy difference between the symmetric and antisymmetric MO's of the bridging ligand, δ, with the angle between the planes of the carboxylato groups of the phthalato dianion, ω.

an ω value of ca. 80°, this latter value being the crystallographic angle between the two carboxylato groups of the phthalato bridge. These results clearly show that the variations in ω should play a significant role on the antiferromagnetic coupling of the complex and/or an ω value of ca. 80° should minimize the antiferromagnetic contribution in the exchange coupling.

Consequently, EHMO calculations could provide a reasonable orbital basis for a qualitative understanding of the relative merit of the ω angle in determining the strength of the magnetic exchange interactions in the phthalato-bridged copper(II) dimers. Moreover, although it is too early for general conclusions to be drawn, it seems probable that a new situation stems leading to ferromagnetic exchange interactions through extended bridging ligands, which is based mainly on the topology of the intervening bridge. More work along this line is under way in our laboratory.

Acknowledgment. We acknowledge Dr. Alain Michalowitcz and Dr. Daniel Andre (Laboratoire de Physico-Chimie Structural, Université Paris Val de Marne, 94000 Creteil, France) for making their Macintosh Ortep[12] version available to us and for their help in using the program. Mac Ortep is available on request, from A.M. and/or D.A.

Supplementary Material Available: Tables SI-SV and SVII, listing a summary of the crystallographic data collection, anisotropic temperature coefficients U_{ij} for the non-hydrogen atoms, atomic parameters for the hydrogen atoms, interatomic distances, bond angles, and experimental and calculated magnetic susceptibility data (9 pages); Table SVI, listing calculated and observed structure factors (20 pages). Ordering information is given on any current masthead page.

Contribution from the Chemical Crystallography Laboratory, University of Oxford, Oxford OX1 3PD, U.K., Department of Chemistry, Northeastern University, Boston, Massachusetts 02115, and Experimental Station, Central Research and Development,[1] E. I. du Pont de Nemours and Company, Wilmington, Delaware 19880-0356

A New Ferric Orthoarsenate Hydrate: Structure and Magnetic Ordering of $FeAsO_4 \cdot {}^3/_4H_2O$

R. J. B. Jakeman,[2a] M. J. Kwiecien,[2b,c] W. M. Reiff,*[,2b] A. K. Cheetham,*[,2a] and C. C. Torardi*[,2d]

Received July 3, 1990

A new hydrated form of $FeAsO_4$ has been synthesized and its crystal structure determined. $FeAsO_4 \cdot {}^3/_4H_2O$ crystallizes in a triclinic cell, $P\bar{1}$, with cell constants a = 6.600 (2) Å, b = 9.015 (2) Å, c = 6.539 (1) Å, α = 104.39 (2)°, β = 104.40 (2)°, γ = 84.25 (2)°, V = 364.7 Å^3, and Z = 4. It exhibits a novel tetrameric unit of iron octahedra, two FeO_6 and two $FeO_5(H_2O)$, that share edges. These units are interconnected by AsO_4 tetrahedra to create a network structure having open channels containing the water molecules bonded to iron as well as water of hydration. Mössbauer spectroscopy measurements over the range T = 298-4.2 K reveal a transition to a three-dimensional magnetically ordered state at ~47.5 K. The Zeeman-split spectra allow for resolution of the two inequivalent iron sites for which internal hyperfine fields of H_n = 535 and 526 kG have been determined at 4.2 K. Magnetic susceptibility measurements indicate antiferromagnetic order below ~49 K in agreement with the Mössbauer spectroscopy results, with the paramagnetic Curie temperature $\Theta \sim -128$ K. The magnetic moment calculated from the Curie-Weiss fit in the paramagnetic region is 5.68 μ_B. The magnitude of $T_{Néel}$ for $FeAsO_4 \cdot {}^3/_4H_2O$ (=$Fe_4(AsO_4)_4 \cdot 3H_2O$) is compared to $T_{Néel}$ for other antiferromagnetically ordered iron(III) arsenate compounds.

Introduction

For several years, we have studied the structures and related magnetic properties of transition-metal compounds containing bridging tetrahedral oxyanions such as PO_4^{3-}, AsO_4^{3-}, SO_4^{2-}, and MoO_4^{2-}. Of these, the compounds of iron have been of special interest and include $Fe_4(OH)_3(PO_4)_3$,[3] layered $FeClMoO_4$ and its alkali-metal insertion compounds,[4] open-framework $Fe_2(SO_4)_3$,[5] and $Fe_2(MoO_4)_3$[6] and its Li insertion compound $Li_2Fe_2(MoO_4)_3$.[7] Such materials are of interest because of their potential as catalysts or as battery materials in electrochemical devices. Prior to our structural determination of anhydrous $FeAsO_4$ by neutron powder diffraction,[8] we tried to grow crystals of this phase by hydrothermal methods. Instead, we isolated a new hydrated form of ferric arsenate having an interesting tunnel arrangement of atoms, which will be discussed in this paper.

The naturally occurring mineral scorodite, $FeAsO_4 \cdot 2H_2O$, is a related hydrated ferric arsenate compound for which Mössbauer spectroscopy,[9,10] magnetic susceptibility,[10] and X-ray crystallog-

(1) Contribution No. 5534.
(2) (a) University of Oxford. (b) Northeastern University. (c) Current address: Gillette Corp., Boston, MA. (d) E. I. du Pont de Nemours and Co.
(3) Torardi, C. C.; Reiff, W. M.; Takacs, L. *J. Solid State Chem.* **1989**, *82*, 203.
(4) Torardi, C. C.; Reiff, W. M.; Lázár, K.; Prince, E. *J. Phys. Chem. Solids* **1986**, *47*, 741.
(5) Takacs, J.; Takacs, L.; Reiff, W. M.; Torardi, C. C. *Hyperfine Interact.* **1988**, *40*, 347.
(6) Battle, P. D.; Cheetham, A. K.; Long, G. J.; Longworth, G. *Inorg. Chem.* **1982**, *21*, 4223.
(7) Reiff, W. M.; Zhang, J. H.; Torardi, C. C. *J. Solid State Chem.* **1986**, *62*, 231.
(8) Cheetham, A. K.; David, W. I. F.; Eddy, M. M.; Jakeman, R. J. B.; Johnson, M. W.; Torardi, C. C. *Nature* **1986**, *320*, 46.
(9) Kiriyama, R.; Sakurai, K. *X-rays* **1949**, *5*, 85; *Struct. Rep.* **1949**, *12*, 251.

0020-1669/91/1330-2806$02.50/0

Table I. Crystallographic Data for $FeAsO_4 \cdot {}^3/_4H_2O$

fw = 208.27	space group $P\bar{1}$ (No. 2)
a = 6.600 (2) Å	T = 20 °C
b = 9.015 (2) Å	λ = 0.71069 Å
c = 6.539 (1) Å	ρ_{calcd} = 3.79 g·cm^{-3}
α = 104.39 (2)°	μ = 136.08 cm^{-1}
β = 104.40 (2)°	transm coeff = 0.5064–0.7116
γ = 84.25 (2)°	$R(F_o)$ = 0.026
V = 364.7 Å^3	$R_w(F_o)$ = 0.036
Z = 4	

Table II. Atomic Positional[a] and Isotropic Thermal Parameters for $FeAsO_4 \cdot {}^3/_4H_2O$ with Esd's in Parentheses

atom	x	y	z	U_{equiv}, Å^2
As(1)	0.99524 (3)	0.68200 (2)	0.80692 (3)	0.00679 (7)
As(2)	1.24838 (3)	0.05716 (2)	0.70795 (3)	0.00576 (7)
Fe(1)	0.86428 (5)	0.30976 (3)	0.64373 (5)	0.0074 (1)
Fe(2)	0.78650 (4)	1.02241 (3)	0.82759 (4)	0.0064 (1)
O(1)	1.1386 (2)	0.7514 (2)	1.0656 (2)	0.0079 (5)
O(2)	0.8973 (3)	0.5166 (2)	0.7960 (3)	0.0148 (7)
O(3)	1.1591 (3)	0.6611 (2)	0.6424 (3)	0.0137 (6)
O(4)	1.1574 (3)	0.2338 (2)	0.6894 (3)	0.0108 (5)
O(5)	1.5020 (3)	0.0637 (2)	0.8220 (3)	0.0139 (6)
O(6)	0.7834 (3)	0.8004 (2)	0.7475 (3)	0.0094 (5)
O(7)	1.2126 (3)	−0.0682 (2)	0.4594 (2)	0.0099 (5)
O(8)	1.1203 (2)	−0.0138 (2)	0.8570 (2)	0.0078 (5)
O(9)	0.5439 (3)	0.3483 (3)	0.5949 (4)	0.0192 (8)
O(10)[b]	0.476 (1)	0.453 (1)	0.017 (2)	0.051 (5)
H(1)	0.487	0.289	0.509	
H(2)	0.502	0.390	0.706	

[a] Space group $P\bar{1}$. [b] Displaced from ($^1/_2$, $^1/_2$, 0) to half-occupied site.

raphy[11,12] results exist. Scorodite also exhibits a tunnel structure where H_2O molecules, bonded to iron, occupy sites in the tunnel. In this investigation, we compare $FeAsO_4$, $FeAsO_4 \cdot {}^3/_4H_2O$ ($Fe_4(AsO_4)_4 \cdot 3H_2O$), and $FeAsO_4 \cdot 2H_2O$. It is shown that variation in the degree of hydration of $FeAsO_4$ has profound effects on the basic structure and strength of magnetic exchange interaction.

Experimental Section

Synthesis. $FeAsO_4 \cdot {}^3/_4H_2O$ ($Fe_4(AsO_4)_4 \cdot 3H_2O$) was prepared under hydrothermal conditions. A typical reaction consisted of sealing 0.8 g of Fe_2O_3 (Alpha 99.9) and 4–5 ml of 4 M H_3AsO_4 solution in a gold tube (15 cm in length × 1 cm in diameter) and heating the mixture at 700–800 °C and 3 kbar pressure for 12 h. The samples were then slowly cooled at a rate of 25 °C/h to 400 °C. The product consisted of a tan polycrystalline powder and light green needle-shaped crystals. The X-ray powder diffraction patterns for both forms were identical and compared quite well with a calculated pattern.[13] This calculated X-ray pattern is provided as a supplementary table.

An isotopically enriched sample, containing 8 times the natural abundance of ^{57}Fe, was prepared from a mixture of Fe_2O_3 and $^{57}Fe_2O_3$. The gold tube container ruptured during this reaction, and although the product contained $FeAsO_4 \cdot {}^3/_4H_2O$ as the major phase, an impurity phase of $FeAs_3O_9 \cdot 8H_2O$ (JCPDS Card No. 22-625) was present. The level of this impurity was estimated to be 10–20% by X-ray powder diffraction.

The title compound was initially characterized by chemical analyses, which gave an Fe:As molar ratio of 0.9. However, thin-crystal microanalysis on a JEOL 100CX Temscan electron microscope showed the crystals to have an Fe:As composition ratio of 1:1 by comparison with a range of iron- and arsenic-containing compounds including $FeAsO_4$. Thermogravimetric analysis showed incipient loss of water at approximately 300 °C that was concluded by 500 °C. Total weight loss observed: 6.5% (calcd 6.48%). Above 900 °C, further loss in weight was seen due to volatile arsenic oxides.

Single-Crystal X-ray Diffraction. Information on the single-crystal X-ray data collection and structural refinement of $FeAsO_4 \cdot {}^3/_4H_2O$ is given in Table I and in a supplementary table. Twenty-five intense diffraction maxima were measured and used to obtain the cell parameters and orientation matrix. The data were treated for Lorentz and polarization effects and averaged in $\bar{1}$ symmetry. An empirical absorption correction was applied.[14] The structure was solved by using the heavy-atom method to locate the As and Fe atoms. Oxygen atoms were found from difference Fourier maps, and a full-matrix least-squares refinement on all non-hydrogen positional and anisotropic thermal parameters was carried out by using the CRYSTALS suite of programs.[15] Oxygen atom O(10), belonging to the water of crystallization, was found displaced from the ($^1/_2$, $^1/_2$, 0) inversion center at (0.476, 0.453, 0.017) and was refined with its occupation fixed at 0.5. Two of the four hydrogen atoms were located from the difference Fourier map. The other two H atoms associated with O(10) were not found.

Positional parameters for $FeAsO_4 \cdot {}^3/_4H_2O$ are given in Table II, important interatomic distances are given in Table III, and bond angles are provided in a supplementary table. Figures were drawn with the assistance of the ORTEP program.[16]

Mössbauer Spectroscopy. Approximately 50 mg of natural-abundance iron-57 $Fe_4(AsO_4)_4 \cdot 3H_2O$ powder was mixed with approximately 25 mg of boron nitride, and the mixture was packed in a thin nylon (12-mm diameter × 3-mm thickness) sample holder. The sample was then mounted in the tail of a flow-type helium-4 cryostat (Supervaritemp Model, Janis Research Co.). Solid or liquid nitrogen was used for the range 298–48 K, and liquid helium was used as the cryogen for the range 48–4.2 K. Temperature control was achieved by using both the calibrated silicon diode/sample-block-heater setup and the nitrogen vapor pressure thermometry/vacuum-regulator setup. The Mössbauer spectra were determined by using a conventional constant-acceleration spectrometer (Canberra Series 35) in conjunction with a Kr/CO_2 gas proportional counter. The γ-ray source was 70-mCi ^{57}Co in a rhodium metal matrix. Curve fitting of the Mössbauer spectra was accomplished by using a program that incorporates statistical goodness-of-fit and reliability tests.[17]

Mössbauer spectroscopy experiments were also carried out for an enriched $Fe_4(AsO_4)_4 \cdot 3H_2O$ powder sample (~15 mg) diluted in boron

Table III. Selected Interatomic Distances (Å) for $FeAsO_4 \cdot {}^3/_4H_2O$ with Esd's in Parentheses

As(1)–O(1)	1.716 (1)	As(2)–O(4)	1.667 (2)
As(1)–O(2)	1.662 (2)	As(2)–O(5)	1.655 (2)
As(1)–O(3)	1.673 (2)	As(2)–O(7)	1.710 (1)
As(1)–O(6)	1.697 (2)	As(2)–O(8)	1.704 (1)
Fe(1)–O(1)	2.111 (1)	Fe(2)–O(1)	2.063 (1)
Fe(1)–O(2)	1.889 (2)	Fe(2)–O(5)	1.870 (2)
Fe(1)–O(3)	1.920 (2)	Fe(2)–O(6)	1.940 (2)
Fe(1)–O(4)	1.962 (2)	Fe(2)–O(7)	2.021 (2)
Fe(1)–O(7)	2.185 (2)	Fe(2)–O(8)	2.162 (1)
Fe(1)–O(9)	2.066 (2)	Fe(2)–O(8′)	2.019 (1)

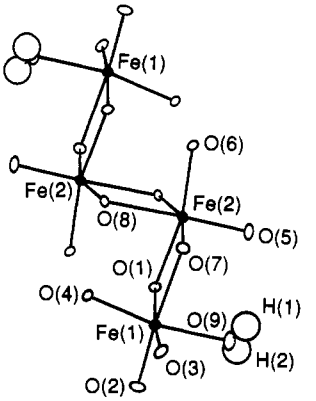

Figure 1. The $Fe_4O_{16}(OH_2)_2$ unit in $FeAsO_4 \cdot {}^3/_4H_2O$ composed of four edge-sharing iron octahedra (ORTEP-drawn with 50% probability anisotropic thermal ellipsoids). An inversion center is located between the Fe(2) atoms.

(10) Takano, M.; Takada, T.; Wada, T.; Okada, K. *J. Phys. Soc. Jpn.* **1971**, *31*, 298.
(11) Kitahama, K.; Kiriyama, R.; Baba, Y. *Acta Crystallogr.* **1975**, *B31*, 322.
(12) Hawthorne, F. C. *Acta Crystallogr.* **1976**, *B32*, 2891.
(13) Yvon, K.; Jeitschko, W.; Parthe, E. *J. Appl. Crystallogr.* **1977**, *10*, 73.
(14) North, A. C. T.; Phillips, D. C.; Mathews, F. S. *Acta Crystallogr.* **1968**, *A24*, 351.
(15) Watki, D. J.; Carruthers, J. R.; Betteridge, P. W. CRYSTALS User Guide; Chemical Crystallography Laboratory, Oxford University: Oxford, U.K., 1985.
(16) Johnson, C. K. ORTEP: A FORTRAN Thermal-Ellipsoid Plot Program for Crystal Structure Illustration; Report 5138; Oak Ridge National Laboratory: Oak Ridge, TN, 1976.
(17) Bancroft, G. M.; Maddock, A. G.; Ong, W. K.; Prince, R. H.; Stone, A. J. *J. Chem. Soc. A* **1967**, 1966.

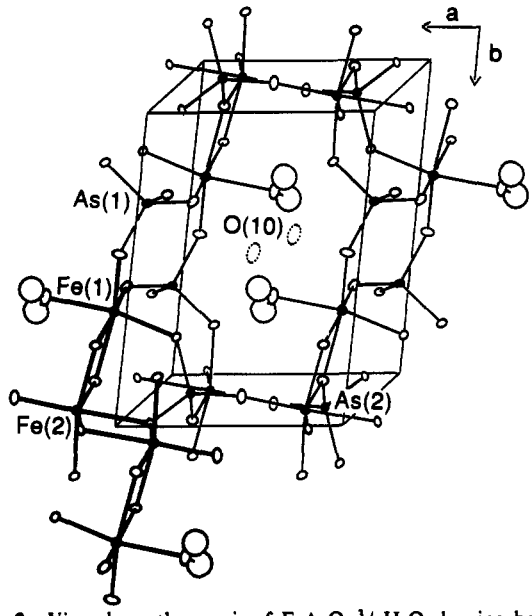

Figure 2. View down the *c* axis of $FeAsO_4 \cdot {}^3/_4H_2O$ showing how the tetrameric iron units are connected by AsO_4 tetrahedra to form a tunnel (ORTEP-drawn with 50% probability anisotropic thermal ellipsoids). H_2O molecules bonded to iron, as well as water of hydration (O(10) drawn with dotted ellipsoids), are found in the tunnels. Fe and As atoms are filled, and one tetrameric $Fe_4O_{16}(OH_2)_2$ unit is highlighted. As(1) atoms are positioned at $y \sim {}^1/_3$ and ${}^2/_3$; As(2) atoms, at $y \sim 0$.

nitride, for which the isotopic enrichment with ^{57}Fe was 16%, i.e., ~8 times natural abundance. Mössbauer spectra obtained for the enriched sample by using the apparatus described above exhibited a dramatic improvement in signal-to-noise ratio in the temperature regime of magnetic hyperfine splitting.

Magnetic Susceptibility. Magnetic susceptibility measurements for $Fe_4(AsO_4)_4 \cdot 3H_2O$ were made on an SHE Co. SQUID magnetometer/susceptometer at the Francis Bitter National Magnet Laboratory, Massachusetts Institute of Technology. A 0.19994-g powder sample was sealed in a KeL-F sample holder that was attached to the sample-transport mechanism. The sample was purged several times with dry helium and lowered into the pickup coil region, which was precooled to 6.0 K. After the sample achieved thermal equilibrium (~1 h), a 5.0-kG field was applied with the superconducting magnet. The susceptometer was operated in computer-control mode and was programmed to collect susceptibility data at 47 temperatures between 301.0 and 6.0 K while maintaining a 5.0-kG field. Six readings were collected at each temperature, and the average value for each temperature constituted one susceptibility data point. Subsequent least-squares curve fitting and plotting were accomplished by using an IBM-XT computer.

Results and Discussion

Crystal Structure. The framework of the $FeAsO_4 \cdot {}^3/_4H_2O$ structure is built of linked FeO_6 octahedra and AsO_4 tetrahedra. A most interesting feature of the structure is the clustering of four FeO_6 octahedra by edge-sharing to form $Fe_4O_{16}(H_2O)_2$ moieties (Figure 1). A center of symmetry is located within this unit between iron atoms Fe(2)···Fe(2). The tetramer contains two kinds of six-coordinate iron, $Fe(1)O_5(H_2O)$ and $Fe(2)O_6$. Average Fe–O bond lengths for Fe(1) and Fe(2), 2.022 and 2.011 Å, compare quite well with the sum of ionic radii[18] for high-spin Fe^{3+} in an oxygen environment, 2.01 Å. Edge-sharing by the iron octahedra causes distortion from a regular geometry, and the edges include the smallest O–Fe–O angles (O(1)–Fe(1)–O(7) = 75.78 (6)°, O(1)–Fe(2)–O(7) = 80.78 (6)°, O(8)–Fe(2)–O(8) = 80.07 (6)°). The shortest Fe–Fe distances are across the shared edges and are 3.242 Å for Fe(1)–Fe(2) and 3.196 Å for Fe(2)–Fe(2). In the mineral pharmacosiderite, $Fe_4(OH)_3(AsO_4)_3 \cdot H_2O$, there are also tetrameric units of edge-sharing FeO_6 octahedra, but the Fe atoms are tetrahedrally arranged so that each Fe octahedron shares an edge with each of the other three octahedra.[19] As in the latter compound, the Fe–O tetramers in $FeAsO_4 \cdot {}^3/_4H_2O$ are interconnected by AsO_4 tetrahedra to form a tunnel structure running along the *c* axis as shown in Figure 2. Both of the crystallographically unique As atoms have regular tetrahedral coordination with average As–O bond lengths of 1.687 Å for As(1) and 1.684 Å for As(2). These bond lengths are similar to those found in other arsenates; the averge As–O bond length in the mineral scorodite, $FeAsO_4 \cdot 2H_2O$, is 1.680 Å.[11]

Each of the eight framework oxygen atoms is connected either to one arsenic and one iron atom with a V-shaped arrangement (O(2) through O(6)) or to one arsenic and two iron atoms with approximately trigonal-planar geometry (O(1), O(7), O(8)). Although the oxygen atoms of the $Fe(2)O_6$ octahedra are all from the basic framework, there are only five framework O atoms bonded to Fe(1). The Fe(1) octahedron is completed by the inclusion of an oxygen atom from an H_2O molecule. These Fe(1)–O(9) bonds are the only ones that point out of the framework into the channel (Figure 2). To satisfy the stoichiometry $Fe_4(AsO_4)_4 \cdot 3H_2O$, one additional H_2O molecule is required per unit cell. The obvious position for this molecule is in the tunnel. One may have suggested that it would be on the inversion center at $({}^1/_2, {}^1/_2, 0)$ because this position would account for the half-occupancy that is required by the stoichiometry, albeit the H atoms would have to be disordered if the O atom was on this site. However, disorder is found in the tunnel, and the O atom of this water molecule is displaced and statistically populating two sites around the inversion center. The occupation of this position is presumably to satisfy the hydrogen-bonding requirement, which is the only bonding that holds this water molecule in place. The $H_2O(9)$ molecule, which is bonded to Fe(1), also forms a hydrogen bond via H(1) across the tunnel to O(6). Also, H(2) of this water molecule hydrogen-bonds to O(10), the water of hydration. The H atoms of the latter must certainly form hydrogen bonds with the framework oxygen atoms; the best candidates appear to be O(2) and O(4). It must be this water of crystallization that is first lost around 300 °C when the compound is heated.

The structure of the other known iron arsenate hydrate with a Fe:As ratio of 1:1, the mineral scorodite, $FeAsO_4 \cdot 2H_2O$, also contains iron octahedra and arsenic tetrahedra,[11] but there are no Fe–O–Fe connections as found for the present compound. Also, each iron atom in the dihydrate has two cis-bonded water molecules pointing into square-shaped tunnels. This hydrate is therefore not structurally related to the new phase discussed above. This is not surprising considering the larger water content of scorodite as compared to $FeAsO_4 \cdot {}^3/_4H_2O$. Anhydrous $FeAsO_4$ has the most condensed structure[8] of the three compounds, as expected, and it is also quite different because it contains pairs of five-coordinated iron atoms that share edges (i.e., Fe_2O_8 units).

Mössbauer Spectroscopy. Zero-field Mössbauer spectra of $Fe_4(AsO_4)_4 \cdot 3H_2O$ were obtained at temperatures between 298 and 49 K for an isotopically unenriched sample and are shown in Figure 3. Spectra with higher signal-to-noise ratios and better resolution were obtained with the enriched sample at temperatures between ~49 and 4.2 K and are shown in Figures 4 and 5. Selected Mössbauer parameters are given in Table IV. At 298 K, the spectrum consists of a slightly asymmetric quadrupole doublet with an isomer shift of +0.32 mm/s, which is reasonable for six-coordinate high-spin Fe^{3+} sites. The quadrupole splitting (ΔE_Q) of 0.47 mm/s is indicative of a slight distortion away from

Table IV. Mössbauer Parameters (mm/s) for $FeAsO_4 \cdot {}^3/_4H_2O$ for $T > T_N$

T, K	isomer shift[a]	quadrupole splitting
298.0	0.322	0.477
78.0	0.382	0.511
49.0	0.460	0.616

[a] Relative to natural iron foil.

(18) Shannon, R. D. *Acta Crystallogr.* **1976**, *A32*, 751.

(19) Buerger, M. J.; Dollase, W. A.; Garaycochea-Wittke, I. *Z. Kristallogr.* **1967**, *125*, 92.

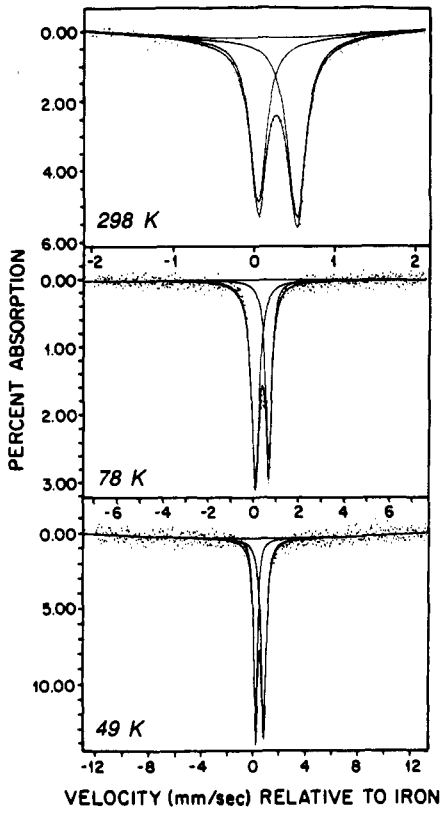

Figure 3. ^{57}Fe Mössbauer spectra for $FeAsO_4 \cdot {}^3/_4H_2O$ (unenriched sample).

perfect octahedral coordination around each of the two Fe(III) sites. The spectra in the paramagnetic temperature range do not, however, resolve the iron inequivalence and cannot be uniquely deconvoluted for the expected four Lorentzians corresponding to two overlapping quadrupole doublets. Similar spectra were obtained at 78 and at 49 K. Ths spectra for 298, 78, and 49 K show a slight asymmetry; however, the direction of the asymmetry is not consistent: the area of the higher energy peak is larger for the 298 and 49 K spectra, and the lower energy peak is larger for the 78 K spectrum. The observed asymmetry behavior may arise from the overlap of two doublets due to the two inequivalent Fe sites, with slightly different quadrupole splitting and temperature dependencies thereof. As stated, it was not possible to resolve two individual doublets from any of the fitted spectra obtained in the paramagnetic state between 298 and 48.75 K, and there is no particular indication of the crystallographically demonstrated iron site inequivalence in the spectral line widths (≈0.35 mm/s).

At ~48 K the Mössbauer spectrum begins to abruptly broaden (Figure 4) and Zeeman-split, indicating the spontaneous magnetization of $Fe_4(AsO_4)_4 \cdot 3H_2O$ and the onset of a transition to a three-dimensional magnetically ordered state. The growth of an internal magnetic field with decreasing temperature resulting in an increased splitting of the Mössbauer spectra is clearly evident, although the magnetically split spectra are complex. At the lowest temperatures studied, 12 or 13 separate transitions are clearly resolved. These spectra appear to consist of two highly overlapped six-line patterns resulting from the two inequivalent iron sites (hereafter referred to as site A and site B), with an additional small doublet (see arrows in Figure 5, $T = 4.2$ K) near the centroid of the sextets ($\delta = 0.45$, $\Delta E_Q = 0.50$ mm/s at 4.2 K) that is due to $FeAs_3O_9 \cdot 8H_2O$, as discussed in the synthesis section.

It appears that the transitions of one hyperfine pattern are nested within the outermost lines of the second sextet (Figures 4 and 5). In Figure 5 ($T = 20.0$ and 4.2 K), the overlap of the two sextets is such that a single line is resolved for the highest velocity transition and two distinct lines were resolved for the lowest velocity transitions. The area under the highest positive-velocity peak is equal to the sum of the areas under the two lowest

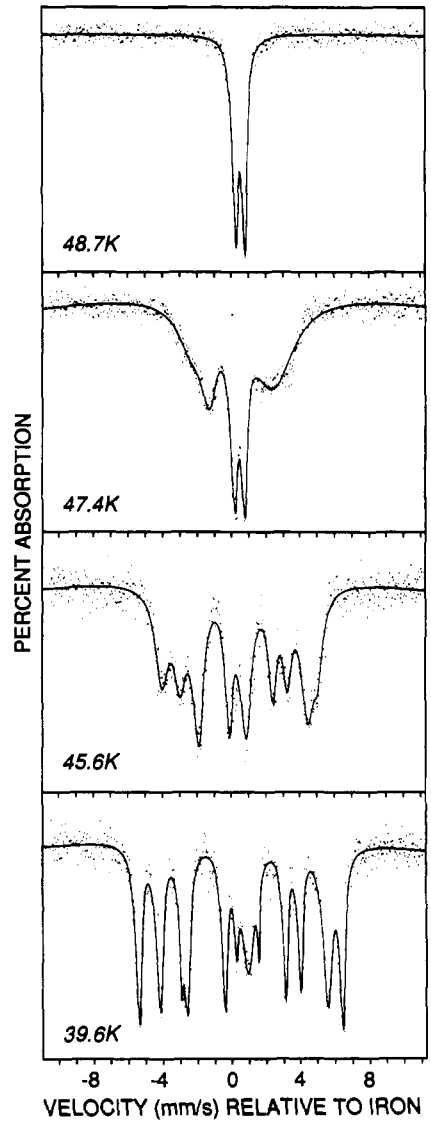

Figure 4. ^{57}Fe Mössbauer spectra for $FeAsO_4 \cdot {}^3/_4H_2O$ (enriched sample).

Table V. Internal Hyperfine Field (H_n) Calculated from Zeeman-Split Mössbauer Spectra for $FeAsO_4 \cdot {}^3/_4H_2O$

T, K	H_n^A, kG	H_n^B, kG	T, K	H_n^A, kG	H_n^B, kG
45.6	282.5	229.7	27.9	480.6	433.1
39.6	369.1	304.8	20.0	516.3	495.5
35.5	450.8	394.3	4.2	534.9	526.2

negative-velocity peaks, which is consistent with the overlapped-sextet interpretation. Using the formula

$$H_n = \Delta_{1-6}(330 \text{ kG})/(10.63 \text{ mm/s}) \quad (1)$$

which neglects any quadrupole shift effects, it was possible to calculate the internal hyperfine field acting on iron sites A and B from the overall splitting of each sextet over the temperature range $T \approx 48$–4.2 K. Table V contains the calculated values of H_n for each site. The internal fields were also calculated by assuming a quadrupole shift in the hyperfine spectrum. Values so obtained agreed with those calculated by using the overall spectral splitting (Δ_{1-6}). This implies that the quadrupole shift effect of the hyperfine patterns is ~0. The rapid onset and smooth increase of internal magnetic fields are evidence for nuclear Zeeman splitting owing to the growth of a molecular field as accompanies cooperative magnetic ordering, as opposed to, e.g., slow paramagnetic relaxation, a single-ion effect. In fact, H_{int} is near 90% of H_{satn} at 30 K. It is clear that site A experiences a larger magnetic field than site B below the ordering temperature (~48 K), although the difference in magnitude between H_n^A and H_n^B decreases as T approaches 4.2 K. H_n^A and H_n^B at 4.2 K are

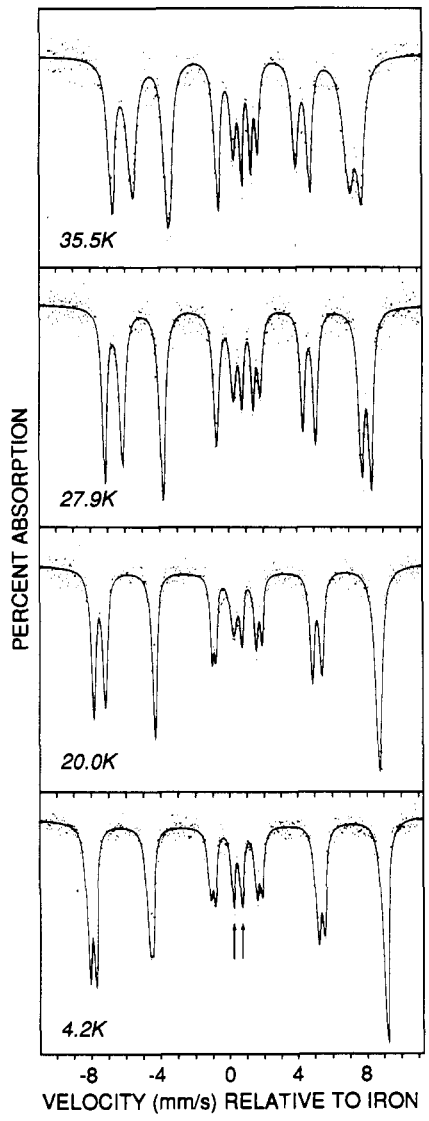

Figure 5. ^{57}Fe Mössbauer spectra for $FeAsO_4 \cdot {}^3/_4H_2O$ (enriched sample).

535 and 526 kG, respectively. These values for H_n are typical for high-spin iron(III) (^{6}A ground term), which, in the absence of orbital and dipolar contributions, has an H_n value of ≈550 kG (i.e., 11 T/unpaired electron, based on the Fermi contact contribution to H_n and neglecting covalency reduction effects). In relation to assigning the observed hyperfine patterns to site A or site B, well-known Mössbauer systematics suggest a larger hyperfine field for a more ionic site.[20] Thus, in view of the data in Table V, it is likely that site A corresponds to the $FeO_5(H_2O)$ site.

Magnetic Susceptibility. Figure 6 (and a supplementary table) summarizes the results of the magnetic susceptibility study of $Fe_4(AsO_4)_4 \cdot 3H_2O$ for polycrystalline samples. The temperature dependence of the molar magnetic susceptibility (χ_M) over the range 6–301 K in a 5.0-kG applied field is shown at the top of Figure 6. A broad maximum is apparent at ~49.0 K, which is evidence for antiferromagnetic ordering. The determination of $T_{Néel}$ from the inflection point of χ_M vs T is ~46 K, which is in reasonable agreement with the 3D magnetic ordering temperature suggested by the Mössbauer spectroscopy data ($T_{Néel} \approx 48$ K). A least-squares fit of inverse susceptibility (χ_M^{-1}) to the Curie–Weiss expression, $\chi_M^{-1} = (T - \Theta)$, over the temperature range 52–300 K at 5.0 kG yields the parameters $C = 4.0$ emu/mol and $\Theta = -128$ K (Figure 6, bottom). The effective moment calculated from this Curie–Weiss fit corresponds to 5.68 μ_B, which is quite

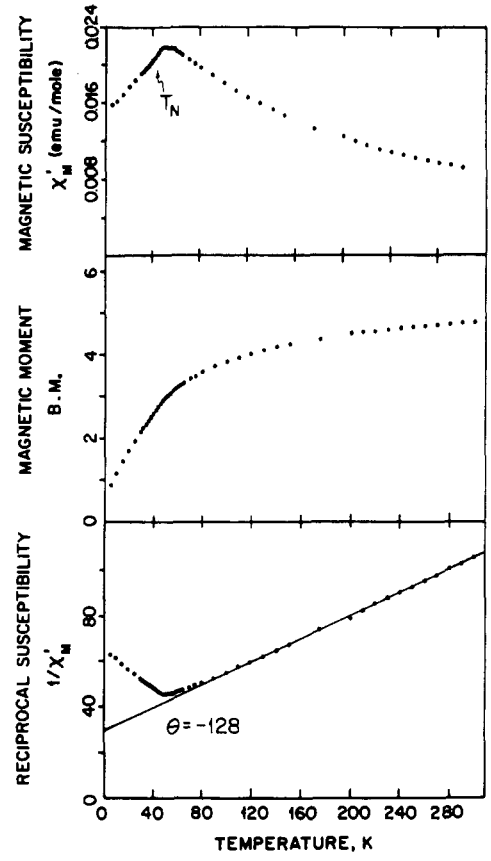

Figure 6. Temperature dependence of molar susceptibility, magnetic moment, and reciprocal susceptibility for $FeAsO_4 \cdot {}^3/_4H_2O$ ($H_0 = 5$ kG).

close to the theoretical value for high-spin iron(III), namely $35^{1/2}$ or 5.92 μ_B. Below the transition temperature (~49 K), χ_M^{-1} deviates from Curie–Weiss behavior in a manner consistent with 3D antiferromagnetic ordering.

Conclusion. The antiferromagnetic ordering of $Fe_4(AsO_4)_4 \cdot 3H_2O$ occurs at a temperature significantly higher than the ordering temperature for the mineral scorodite, $FeAsO_4 \cdot 2H_2O$, which antiferromagnetically orders below ~17 K, and at a temperature somewhat lower than that for anhydrous $FeAsO_4$, $T_{Néel} \approx 67$ K.[21] One cannot make meaningful direct comparisons of these materials owing to their rather different structures. However, a basic view of these systems is that each is a network of interacting Fe^{3+} ions containing either zero, three-fourths, or two water molecules per $FeAsO_4$ unit. For this series of iron arsenates then, there is a trend toward lower ordering temperatures (i.e., weaker magnetic exchange interactions) with increasing water content. We know of no other iron(III) arsenate network systems for further useful comparisons to those discussed herein. In any event, one would expect diamagnetic water molecules to "dilute" the magnetic lattice, since coordinated water oxygens do not directly bridge magnetic centers in the lattice. Thus, in *anhydrous* $FeAsO_4$, where each iron is coordinated to five oxygens (two oxygens are involved in Fe–O–Fe dimer bridges, and the remaining three are part of the AsO_4 tetrahedra, which bridge the iron dimers), magnetic exchange through the bridging (–O– or –O–As–O–) network is relatively strong, and $T_{Néel}$ is relatively high. In $Fe_4(AsO_4)_4 \cdot 3H_2O$, one of the two iron sites is octahedrally coordinated by framework oxygens, and the other site is coordinated by five framework oxygens and *one water oxygen*. Coordination of the nonbridging diamagnetic water molecule results in a structure that is less magnetically condensed than the anhydrous $FeAsO_4$ network and, as expected, exhibits a lower ordering temperature. Finally, in the mineral scorodite, each iron octahedron is coordinated with *two water oxygens*, with the remainder of the coordination pos-

(20) Greenwood, N. N.; Gibb, T. C. Mössbauer Spectroscopy; Chapman and Hall Ltd.: London, 1971; p 151.

(21) Kwiecien, M. J.; Reiff, W. M.; Jakeman, R. J. B.; Cheetham, A. K.; Torardi, C. C. In preparation.

itions again occupied by framework oxygen atoms from bridging AsO_4 tetrahedra. This network is apparently even less magnetically condensed than either of the foregoing iron arsenates and, accordingly, exhibits a significantly lower magnetic ordering temperature.

Acknowledgment. W.M.R. acknowledges support by the U.S. National Science Foundation Division of Materials Research Solid State Chemistry Program and by the Northeastern University RSDF and Biomedical Research Support Fund for the purchase of the ^{57}Co Mösssbauer spectroscopy source.

Supplementary Material Available: Tables giving anisotropic thermal parameters, the calculated X-ray powder diffraction pattern, full crystallographic information, interatomic distances and angles, and magnetic susceptibility data and figures of Mössbauer spectra including all Lorentzian fits (9 pages); a listing of observed and calculated structure factors (17 pages). Ordering information is given on any current masthead page.